The role of malignant tissue on the thermal distribution of cancerous breast

The role of malignant tissue on the thermal distribution of cancerous breast

Ariel Ramírez-Torres[a], Reinaldo Rodríguez-Ramos[b], Federico J. Sabina[c], Catherine García-Reimbert[c], Raimondo Penta[d], José Merodio[d], Raúl Guinovart-Díaz[b], Julián Bravo-Castillero[b], Aura Conci[e], Luigi Preziosi[a]

[a]*Dipartimento di Scienze Matematiche "G. L. Lagrange", Politecnico di Torino, 10129. Torino, Italia*
[b]*Departamento de Matemáticas, Facultad de Matemática y Computación, Universidad de La Habana, CP 10400, La Habana, Cuba*
[c]*Instituto de Investigaciones en Matemáticas Aplicadas y en Sistemas (IIMAS), Universidad Nacional Autónoma de México, 01000 CDMX, Apartado Postal 20-126, México*
[d]*Departamento de Mecánica de los Medios Continuos y T. Estructuras, E.T.S. de Caminos, Canales y Puertos, Universidad Politécnica de Madrid, CP 28040, Madrid, España*
[e]*Instituto de Computação, Universidade Federal Fluminense, CEP:24210-346. Río de Janeiro, Brasil*

Abstract

The present work focuses on the integration of analytical and numerical strategies to investigate the thermal distribution of cancerous breasts. Coupled stationary bioheat transfer equations are considered for the glandular and heterogeneous tumor regions, which are characterized by different thermophysical properties. The cross-section of the cancerous breast is identified by a homogeneous glandular tissue that surrounds the heterogeneous tumor tissue, which is assumed to be a two-phase periodic composite with non-overlapping circular inclusions and a square lattice distribution, wherein the constituents exhibit isotropic thermal conductivity behavior. Asymptotic periodic homogenization method is used to find the effective properties in the heterogeneous region. The tissue effective thermal conductivities are computed analytically and then used in the homogenized model, which is solved numerically. Results are compared with appropriate experimental data reported in the literature. In particular, the tissue scale temperature profile agrees with experimental observations. Moreover, as a novelty result we find that the tumor volume fraction in the heterogeneous zone influences the breast surface temperature.

Keywords: heterogeneous breast cancer, thermography, asymptotic homogenization

1. Introduction

Breast cancer is the leading cause of cancer death among US 20-59 years-old woman [1]. In recent years, an increasing number of prospective studies focusing on this disease have emerged. Actually, some clinical protocols are employed to detect and provide a diagnosis of breast cancer, such as ultrasound, mammography, thermography, among others. Mammography is the imaging test most widely employed for the detection of breast cancer, however it has a range of known limitations. For instance, it is less sensitive in detecting tumors in woman with dense breast tissue and implants, there is a risk of rupture of tumor's encapsulation (as the process of taking a mammogram involves the compression of the breast tissue) and also, confers a slightly increased risk of causing radiation induced breast cancer [2]. On the

other hand, breast ultrasound technique has been considered a useful tool in dense breasts. Nevertheless, many cancers are not visible to ultrasound and its accuracy has been found to depend on three factors: quality of the tools, expertise of the physician and the use of physically multiple approaches for breast cancer detection (e.g. thermography combined with ultrasound and biopsy) [2, 3, 4]. Nowadays, thermography technique has emerged as a prospective method to complement mammography and to improve the efficiency of breast cancer early and overall detection [3, 5]. Breast infrared thermography is a noninvasive procedure that does not involve compression of the breast tissue or exposure to radiation, and works through an assessment of physiological functions, through high resolution surface temperature measurements ([6]). Particularly, an abnormal thermogram has been shown to be a reliable prognostic indicator of increased risk of breast cancer at early stage [7, 8]. In addition, many researchers advocate that thermography ought to be performed more frequently and in between mammography cycles, since the latter uses radiation which is harmful to the body. The breast thermography for cancer detection is justified by the fact that tumor growth causes angiogenesis-dependence and this neo-vascularization causes an increase in temperature in the region near the tumor.

Thermography, because it is a thermal picture of the skin, is unable to localize a lesion or tumor since abnormalities found by infrared imaging do not define an area that can be surgically biopsied. The interpretation of the thermal images relies on the identification of areas of increased temperature, making areas of low metabolic activity or "cold" tumors more difficult to identify. Then, in order to complement the breast tumor detection by infrared imaging techniques, mathematical models have been proposed to estimate the temperature distribution over breasts with and without tumors. Particularly, several works model heat transfer in a biological tissue using the Pennes bioheat equation. For instance, in [9] the effect of changing the breast density composition to its surface temperature distribution profile was investigated. The effect of thermal and elastic properties on the breast surface temperature distribution was investigated in [10] by means of the finite element method (FEM). Moreover, in [11] the presence of a tumor and the estimation of its size and location in a tissue was studied via FEM. A standardized protocol for the acquisition of breast thermal images was developed in [3], including the design, construction and installation of the mechanical apparatus. A methodology for estimating thermal properties based on such infrared images was presented, where the physical process was governed by the static bioheat transfer equation.

In order to improve and extend the knowledge of cancerous breast thermal distribution, we consider the cross-section of a breast to be with an embedded malignant heterogeneity region defined as a two-phase periodic composite with non-overlapping circular inclusions and a square lattice distribution, wherein the constituents exhibit isotropic thermal conductivity behavior. In previous works, soft tissues assume to present a similar type of arrangement. For example, in [12], a porous tissue microstructure is depicted with an alike periodic geometry. Several works adopt the typical convention of treating the entire cancerous region as a homogeneous one. Here, the heterogeneity of the tumor is taken into account, suiting up a more realistic condition. A novel semi-analytical approach to overcome the problem is then proposed. That is, analytical and finite element computations are integrated to solve the stationary bioheat transfer equation. We apply the asymptotic homogenization technique [13, 14] exploiting the sharp length scale separation between the local malignant hetereogeneities and the characteristic size of the whole tissue. We compute the macroscale thermal conductivities solving the local cell problem analytically [15], [16] for the primary cancer and we solve it in macro-scale via finite element method. Moreover, the methodology used at the lower length scale (i.e. in

tumorous region) assumes the cancer has a periodical primary growing (i.e. before to form multiple secondary cancers or metastases). This is used because it is a frequent biological assumption according the cancer pre-metastatic behavior and even when it is spreading in most of the cases. Finally we consider that the tumor grade cannot be assessed and that it is a well differentiated one. These are the most common types of cancers and include soft tissue sarcoma, primary brain tumor, prostate and breast cancer. In our results, we found that the degree of cancer volume fraction in the cancerous region affects the breast surface temperature, i.e. more cancerous tissue volume fraction induces an increase in the breast surface temperature. This new modeling approach provides qualitative and quantitative hints that can potentially be used to improve tumor detection based on temperature maps of the breast tissue.

The work is organized as follows. In Section 2, the geometry for representing the breast is described. In Section 3 the mathematical model for finding the breast temperature profile is stated, where the static version of the bioheat transfer equation (BHTE) as proposed by [17] is used. In Section 4 the homogenization procedure is illustrated, where the homogenized equation and the effective coefficients are obtained. In Section 5 the method to find the solution is described and in Section 6 the numerical results are presented and discussed. Finally, conclusions are presented in section 7.

2. Physical model

Fibroadenoma is the most common surgically treated breast mass in adolescents, accounting for 44 to 94% of biopsied breast lesions [18]. It is a benign tumor made of glandular and fibrous tissue [19] which is encapsulated and round. Even if it is unusual for a breast carcinoma to arise within a fibroadenoma, there are many reported cases in the literature where *in situ* ductal carcinoma has been identified inside it [20, 21, 22]. Moreover, it has been found out that fibroadenomas raise the temperature so that it can be detected using thermal imaging [23]. Given the above biological scenario, a two-dimensional cross-section of the average female breast geometry is considered, composed of glandular tissue and the tumor lesion is assumed to be an encapsulated and round heterogeneous tissue composed of both glandular and periodically arranged circular cancerous inclusions (Fig. 1). It is also assumed to be hemispherically shaped with a diameter $L = 0.14$ m. In fact, in [12], it is claimed that a periodic (porous) microstructure could represent a malignant cell aggregate.

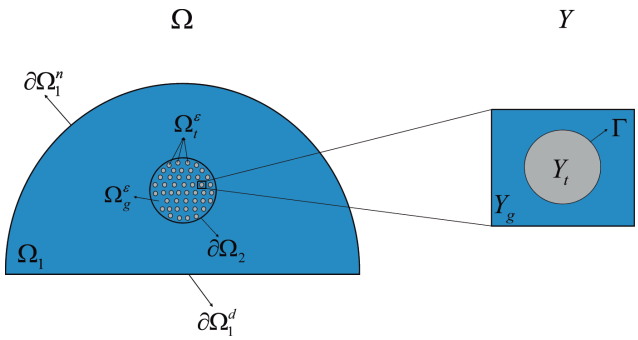

Figure 1: Decomposition of the macroscopic domain (left) and the corresponding unit periodic cell (right).

The homogeneous tissue (assumed to be glandular tissue) surrounding the tumor region is associated with the open, bounded and connected domain Ω_1 with Lipschitz boundary

$\partial\Omega_1 = \partial\Omega_1^n \cup \partial\Omega_1^d$ and $\partial\Omega_1^n \cap \partial\Omega_1^d = \emptyset$. The composite cancerous tissue is supposed to be surrounded by the homogeneous tissue and characterized by two regions of different thermophysical properties: the cancerous inclusions (Ω_t^ε) and the square lattice of glandular tissue (Ω_g^ε) where Ω_g^ε is connected. In this sense, the cancerous region will consist of a periodic microstructure associated with the open, bounded and connected domain $\Omega_2 = \Omega_g^\varepsilon \cup \Omega_t^\varepsilon \cup \partial\Omega_2$ with Lipschitz boundary $\partial\Omega_2$ and with $\Omega_g^\varepsilon \cap \Omega_t^\varepsilon = \emptyset$. Then, the cancerous breast is represented by $\Omega = \Omega_2 \cup \Omega_1$. Let $\varepsilon > 0$ be the size of the microstructure and introduce the fast scale coordinate $\mathbf{y} = \mathbf{x}/\varepsilon$. The reference periodic cell will be denoted by Y, which contains one inclusion occupying the domain Y_t such that $Y = Y_g \cup Y_t \cup \Gamma$, with $\overline{Y}_t \subset Y$ and $Y_g \cap Y_t = \emptyset$.

Table 1 lists the symbols used in this work.

Table 1: Notation

Symbol	Description
$\lvert \bullet \rvert$	Volume fraction of $\bullet$
$[\![\bullet]\!]$	Contrast across the interface taken from the matrix to the inclusions
$\langle\bullet\rangle$	Volume average over the periodic cell
ε	Small parameter
ρ_b	Blood mass density
c_b	Blood specific heat capacity
ω_b	Blood perfusion
q_m	Metabolic heat generation
h	Combined effective heat transfer coefficient due to convection, radiation and evaporation
u_e	Surrounding temperature
u_a	Arterial blood temperature
u_c	Boundary temperature between the breast and the chest
u	Temperature
$\mathbf{x}$	Macroscopic (or slow) scale
$\mathbf{y}$	Microscopic (or fast) scale
Y	Reference unit periodic cell
Y_g	Glandular tissue in the reference unit periodic cell
Y_t	Tumoral tissue inclusion in the reference unit periodic cell
Ω	Breast domain
Ω_1	Breast domain without the tumorous region
Ω_2	Heterogeneous tumorous domain
Ω_g^ε	Glandular tissue within heterogeneous tumorous domain
Ω_t^ε	Tumoral tissue within heterogeneous tumorous domain
$\mathbf{K}$	Thermal conductivity tensor

3. Statement of the problem

The objective of the paper is to find the stationary temperature fields u and u^ε that are described by a coupled stationary Penne's bioheat transfer equations [17], which are heat conduction equations including the effect of blood flow in tissue temperature on a continuum basis, with specific terms for the generation of heat due to blood perfusion and for metabolic heat.

In the homogeneous tissue (the glandular region surrounding the tumor heterogeneity) the problem reads as,

$$(\mathcal{P}^g)\begin{cases} -\nabla\cdot(\mathbf{K}^g\nabla u)+\rho_b c_b\omega_b^g\,(u-u_a)=q_m^g & \text{in } \Omega_1,\\ -\mathbf{K}^g\nabla u\cdot\mathbf{n}=h\,(u-u_e) & \text{on } \partial\Omega_1^n,\\ u=u_c & \text{on } \partial\Omega_1^d. \end{cases} \tag{1}$$

Problem $(\mathcal{P}^g)$ is already set in a macro-scaled framework, because there are no heterogeneities and as such, there is not need to obtain an equivalent representation of it. On the other hand, in the heterogeneous tissue (the cancerous area), the problem is defined as follows,

$$(\mathcal{P}^\varepsilon)\begin{cases} -\nabla\cdot(\mathbf{K}^\varepsilon\nabla u^\varepsilon)+\rho_b c_b\omega_b^\varepsilon\,(u^\varepsilon-u_a)=q_m^\varepsilon & \text{in } \Omega_2,\\ \mathbf{K}^\varepsilon\nabla u^\varepsilon\cdot\mathbf{n}=\mathbf{K}^g\nabla u\cdot\mathbf{n} & \text{on } \partial\Omega_2,\\ u^\varepsilon=u & \text{on } \partial\Omega_2. \end{cases} \tag{2}$$

In (1) and (2), superscripts $\bullet^g$ and $\bullet^\varepsilon$ are used to indicate the belonging to Ω_1 or Ω_2, respectively. Moreover, the rapidly oscillating material properties $\mathbf{K}^\varepsilon$, ω_b^ε and q_m^ε, are given as piecewise constant functions,

$$\mathbf{K}^\varepsilon(\mathbf{x})=\begin{cases} k_g\mathbf{I} & \mathbf{x}\in\Omega_g^\varepsilon,\\ k_t\mathbf{I} & \mathbf{x}\in\Omega_t^\varepsilon, \end{cases},\quad \omega_b^\varepsilon(\mathbf{x})=\begin{cases} \omega_b^g & \mathbf{x}\in\Omega_g^\varepsilon\\ \omega_b^t & \mathbf{x}\in\Omega_t^\varepsilon \end{cases}\quad\text{and}\quad q_m^\varepsilon(\mathbf{x})=\begin{cases} q_m^g & \mathbf{x}\in\Omega_g^\varepsilon,\\ q_m^t & \mathbf{x}\in\Omega_t^\varepsilon. \end{cases}$$

Boundary conditions for $(\mathcal{P}^g)$ are heat transfer by convection between the surface of the tissue and the external environment on $\partial\Omega_1^n$ and a prescribed temperature on $\partial\Omega_1^d$. In the case of $(\mathcal{P}^\varepsilon)$ we assume heat flux and temperature continuity. In the same way, continuity conditions for heat flux and temperature are imposed on Γ, i.e.,

$$[\![u^\varepsilon]\!]=0\quad\text{and}\quad[\![\mathbf{K}^\varepsilon\nabla_x u^\varepsilon\cdot\mathbf{n}]\!]=0\qquad\text{on }\Gamma, \tag{3}$$

where $[\![\bullet]\!]=\bullet_g-\bullet_t$.

In Section 4, we deal with problem $(\mathcal{P}^\varepsilon)$ via asymptotic homogenization technique in order to obtain a homogenized representation of it (denoted by $(\mathcal{P}^h)$). Macroscale boundary conditions are found for the homogenized problem allowing us to coupled it with $(\mathcal{P}^g)$. Finally, after finding the effective coefficient of the homogenized problem via an analytical procedure, we merged the coupled macro problems (that is $(\mathcal{P}^g)$ and $(\mathcal{P}^h)$) into a single one and solve it numerically.

4. Homogenization procedure

In order to obtain an homogenized formulation of $(\mathcal{P}^\varepsilon)$ in the heterogeneous tissue Ω_2, the two-scale homogenization technique is employed. The basic theory of the homogenization method can be found in [13, 14]. Then, an asymptotic expansion of u^ε is sought as a function of ε for $\varepsilon\to 0$ in the form

$$u^\varepsilon(\mathbf{x})=u_0(\mathbf{x},\mathbf{y})+\varepsilon u_1(\mathbf{x},\mathbf{y})+\varepsilon^2u_2(\mathbf{x},\mathbf{y})+\ldots, \tag{4}$$

where the functions $u_i(\mathbf{x},\mathbf{y})$ are Y-periodic in $\mathbf{y}$.

Remark 1 (On the periodicity assumption and macroscopic uniformity)**.** *The arragement of cancerous inclusions is in general non-periodic, and the assumption of local periodicity is technically enforced to carry out the standard asymptotic homogenization steps in order to obtain a tissue scale formulation of the problem, as done in this section. This way, we are able to restrict our microstructural analysis to a single portion (i.e. the cell) of the domain, where we are to solve differential problems (numerically and/or analytically) in practice. However, the periodic cell itself is not necessarily the same for each macroscale point* $\mathbf{x}$*, and our formulation could be extended to such* non-macroscopically uniform *media to account for given, realistic arragements of cancerous inclusions provided by clinical measurements. This generalization would lead to slight modifications of the resulting tissue scale equations (due to variations of the periodic cell with respect to the macroscale variable* $\mathbf{x}$*), and to a much more complex computational procedure, which would require the solution of different cell problems at each macroscale point, as depicted in detail in the context of porous and poroelastic media, for example in [24, 25, 26, 12]. Here, we thus focus on the particular case of* macroscopic uniformity *(i.e. accounting for a periodic cell which is independent of* $\mathbf{x}$*) for the sake of simplicity, as we aim at providing a first modeling step which can qualitatively match the available literature results.* □

The fact that

$$\mathbf{y} = \frac{\mathbf{x}}{\varepsilon},$$

implies that

$$\nabla \to \nabla_x + \varepsilon^{-1}\nabla_y, \tag{5}$$

where ∇_j indicates that the derivative is taken with respect to $j = x, y$. The substitution of expansion (4) into problem $(\mathcal{P}^\varepsilon)$ and using the chain rule (5) leads to a sequence of problems in powers of ε to be solved.

(i) To $O(\varepsilon^{-2})$,

$$-\nabla_y \cdot (\mathbf{K}^\varepsilon \nabla_y u_0) = 0.$$

Then, applying the solvability condition in [14] to the last equation, i.e. like the average of the right hand side is zero, it is deduced that,

$$u_0(\mathbf{x}, \mathbf{y}) = u_0(\mathbf{x}). \tag{6}$$

(ii) To $O(\varepsilon^{-2})$ and using result (6), we can write

$$-\nabla_y \cdot (\mathbf{K}^\varepsilon \nabla_y u_1) = \nabla_y \cdot (\mathbf{K}^\varepsilon \nabla_x u_0)\,.$$

Then, by the $\mathbf{y}$-periodicity of $\mathbf{K}^\varepsilon$ and the solvability condition, the last equation has a $\mathbf{y}$-periodic solution which is unique up to an additive constant. In particular, since the problem is linear and u_0 only depends on $\mathbf{x}$, then u_1 can be written as $u_1(\mathbf{x}, \mathbf{y}) = \boldsymbol{\chi}(\mathbf{y}) \cdot \nabla_x u_0(\mathbf{x})$, where $\boldsymbol{\chi}(\mathbf{y})$ is a periodic vector function in $\mathbf{y}$ with $\langle \boldsymbol{\chi} \rangle = 0$ ($\langle \bullet \rangle$ denotes the volume average over the periodic cell), satisfying the local problem

$$\begin{cases} -\nabla_y \cdot (\mathbf{K}^\varepsilon \nabla_y (\boldsymbol{\chi} + \mathbf{y})) = 0, & \text{in } Y \setminus \Gamma \\ [\![\boldsymbol{\chi}]\!] = 0, & \text{on } \Gamma \\ [\![(\mathbf{K}^\varepsilon \nabla_y (\boldsymbol{\chi} + \mathbf{y})) \cdot \mathbf{n}]\!] = 0, & \text{on } \Gamma \end{cases} \tag{7}$$

(*iii*) To $O(\varepsilon^0)$, using result (6) and substituting the above form of u_1, we have

$$-\nabla_x \cdot (\mathbf{K}^\varepsilon \nabla_x u_0) - \nabla_x \cdot (\mathbf{K}^\varepsilon \nabla_y \boldsymbol{\chi} \nabla_x u_0) - \nabla_y \cdot (\mathbf{K}^\varepsilon \chi \nabla_x u_0) - \nabla_y \cdot (\mathbf{K}^\varepsilon \nabla_y u_2) + g^\varepsilon u_0 = f^\varepsilon,$$

where $g^\varepsilon = \rho_b c_b \omega_b^\varepsilon$ and $f^\varepsilon = q_m^\varepsilon + \rho_b c_b \omega_b^\varepsilon u_a$. Applying the volume average operator to the last equation and using the $\mathbf{y}$-periodicity of the involved functions, it is obtained that $u_0(\mathbf{x})$ is the solution of the homogenized problem

$$(\mathcal{P}^h) \begin{cases} -\nabla_x \cdot \left(\hat{\mathbf{K}} \nabla_x u_0 \right) + \langle g^\varepsilon \rangle \, u_0 = \langle f^\varepsilon \rangle, & \text{in } \Omega_2 \\ \hat{\mathbf{K}} \nabla_x u_0 \cdot \mathbf{n} = \mathbf{K}^g \nabla_x u \cdot \mathbf{n}, & \text{on } \partial\Omega_2 \\ u_0 = u, & \text{on } \partial\Omega_2 \end{cases} \tag{8}$$

where

$$\hat{\mathbf{K}} = \langle \mathbf{K}^\varepsilon + \mathbf{K}^\varepsilon \nabla_y \boldsymbol{\chi} \rangle \tag{9}$$

denotes the effective coefficient and

$$\langle g^\varepsilon \rangle = \rho_b c_b \omega_b^g \frac{|Y_g|}{|Y|} + \rho_b c_b \omega_b^t \frac{|Y_t|}{|Y|} \quad \text{and} \quad \langle f^\varepsilon \rangle = \left(q_m^g + \rho_b c_b \omega_b^g u_a \right) \frac{|Y_g|}{|Y|} + \left(q_m^t + \rho_b c_b \omega_b^t u_a \right) \frac{|Y_t|}{|Y|}.$$

In summary, an equation, whose coefficient is not rapidly oscillating is obtained, while its solution is close to that of the original problem. This is the homogenized equation and its coefficient represents the macroscopic effective property of the composite.

5. Solution of the problem

We need to solve problems $(\mathcal{P}^g)$ and $(\mathcal{P}^h)$. In fact, by introducing the characteristic functions $\Phi_i \in \Omega_i$ $(i = 1, 2)$, namely

$$\Phi_i = \begin{cases} 1 & \text{if } \mathbf{x} \in \Omega_i \\ 0 & \text{if } \mathbf{x} \notin \Omega_i \end{cases}$$

and defining

$$\mathbf{K} = \mathbf{K}^g \Phi_1 + \hat{\mathbf{K}} \Phi_2, \quad G = g\Phi_1 + \langle g^\varepsilon \rangle \, \Phi_2 \quad \text{and} \quad F = f\Phi_1 + \langle f^\varepsilon \rangle \, \Phi_2,$$

where $g = \rho_b c_b \omega_b^g$ and $f = q_m^g + \rho_b c_b \omega_b^g u_a$. Both, $(\mathcal{P}^g)$ and $(\mathcal{P}^h)$, can be merged into one single problem as follows,

$$(\mathcal{P}) \begin{cases} -\nabla \cdot (\mathbf{K} \nabla u) + G u = F & \text{in } \Omega, \\ -\mathbf{K}^g \nabla u \cdot \mathbf{n} = h \, (u - u_e) & \text{on } \partial\Omega_1^n, \\ u = u_c & \text{on } \partial\Omega_1^d. \end{cases} \tag{10}$$

Then, the following procedure is adopted in order to solve (10).

(i) Solve the cell problem

The first step consists in solve the cell problem (7). Here, we adopt the procedure and results given by [15, 16] adapting it to the thermal case. In these papers, the theory of analytical functions ([27]) was applied to solve the cell problem. The solutions of the local problems are written as (see Appendix A)

$$\chi_1^{(g)} = \mathcal{R}\left\{a_0^1 z + \sum_{l=1}^{\infty\ o} a_l^1 \frac{\zeta^{(l-1)}(z)}{(l-1)!}\right\} \quad \text{and} \quad \chi_1^{(t)} = \mathcal{R}\left\{\sum_{l=1}^{\infty\ o} c_l^1 z^l\right\}, \tag{11}$$

$$\chi_2^{(g)} = \mathcal{I}\left\{a_0^2 z + \sum_{l=1}^{\infty\ o} a_l^2 \frac{\zeta^{(l-1)}(z)}{(l-1)!}\right\} \quad \text{and} \quad \chi_2^{(t)} = \mathcal{I}\left\{\sum_{l=1}^{\infty\ o} c_l^2 z^l\right\}, \tag{12}$$

where the aim is to find the real coefficients a_l^p and c_l^p. The interphase conditions in (7) lead to the solution of the following infinite linear system for each problem defined by $p = 1, 2$

$$\left(\mathbf{I} + (-1)^{p+1}\xi \mathbf{W}^p\right)\hat{\mathbf{A}}^p = \mathbf{V}^p, \tag{13}$$

with $\hat{\mathbf{A}}^p = (\hat{a}_1^p, \hat{a}_2^p, \ldots)^T$, $\hat{a}_k^p = a_k^p\sqrt{k}/R^k$, $\mathbf{V}^p = ((-1)^{p+1}\xi R, 0, \ldots)^T$, $\xi = \frac{k_g - k_t}{k_g + k_t}$ and

$$\mathbf{W}^p = \begin{cases} (-1)^{p+1}\pi R^2 & \text{for } k + l = 2, \\ \sum\limits_{k=1}^{\infty\ o} \sqrt{kl}\eta_{kl} R^{k+l} & \text{for } k + l > 2. \end{cases}$$

(ii) Find the homogenized coefficient

In order to determine the effective properties $\hat{K}_{ik}$, it is necessary to truncate the system (13) into an appropriate order $k = N$. In fact, only a_1^p will be needed. Indeed if $p = 1$, using the form of $\mathbf{K}$, Green's theorem and the double periodicity of χ_1

$$\hat{K}_{11} = k_t\left|Y_t\right| + k_g\left|Y_g\right| - (k_t - k_g)\int_\Gamma \chi_1^{(g)} \mathrm{d}y_2.$$

Now, using the orthogonality properties of the trigonometric functions $\{\sin\theta l, \cos\theta l\}$ and relations (A.7)-(A.9) of the Appendix A,

$$\hat{K}_{11} = k_g\left(1 - 2\pi a_1^1\right). \tag{14}$$

Analogously, for $p = 2$

$$\hat{K}_{22} = k_t\left(1 + 2\pi a_1^2\right). \tag{15}$$

If $k_g = k_t$, then $\hat{K} = \hat{K}_{11} = \hat{K}_{22} = k_g$.

(iii) Solve $(\mathcal{P})$

Finally, once we found the effective coefficient we can solve problem (10). For this purpose we use *FreeFem++*. In particular, we approximate the involved functions by piecewise linear continuous finite elements. Moreover, the existence, uniqueness and regularity of the problem weak solution (10) can be proved by standard methods using the Lax-Milgram theorem.

6. Numerical solution and discussion of the results

In the present section, the breast surface temperature change due to a given localized cancerous tissue in an otherwise healthy breast tissue is studied. Numerical calculations were carried out for two breast models A and B, whose tissue parameters, shown in Tab. 2, were taken from [3] and [28], respectively. The data cited in Tab. 2 for the tumor and the glandular tissues

Table 2: Tissue parameters

	[3] (Model A)	**[28]** (Model B)
k_g (W/m ℃)	0.48	0.48
k_t (W/m ℃)	0.48	0.511
ω_b^g (1/s)	0.00018	0.000539
ω_b^t (1/s)	0.009	0.0108
c_b (J/kg ℃)	4200	4200
ρ_b (kg/m^3)	1060	1060
q_m^g (Wm^{-3})	450	700

(thermal conductivity, blood perfusion) refer to the specific portion they occupy in Ω_2 and not the entire tumor region. Moreover, temperatures are fixed as $u_a = u_c = 37$℃ [29] and h is set to 13.5 W/m ℃ [9]. Now, thermograms are sensitive to environmental changes in temperature, humidity and air circulation, so they need to be captured under strict protocols. In this sense, the patient is usually required to rest for 10-20 minutes with clothing removed from the relevant area to achieve thermal equilibrium in a room at 18-22℃ [29]. In this sense, the surrounding temperature is fixed to $u_e = 20$℃. The metabolic heat value for different tumor sizes follows the law given in [10] as $q_m^t = C/(468.6\ln(100D) + 50)$, where $C = 3.27 \times 10^6$ Wday/m^3 and D is the tumor diameter.

The *in vivo* experiments conducted by [30] on breast tumors permitted to estimate the mean effective thermal conductivity. In their results, thermal conductivity of cancer tissue was higher than that of healthy tissue, the latter being approximately twice as high for glandular tissue as for fat tissue. In particular, it was measured an enhancement in conductivity due to blood perfusion, as 0.511 W/m℃. In fact, it has long been revealed that blood perfusion in the tumor area often appear abnormally high with respect to the surrounding tissue [29]. In the data presented in Tab. 2, we observe that tumor blood perfusion by [28] is higher than that from [3], which induces an increase in the thermal conductivity of the cancerous tissue. The intramammary measurements of thermal conductivity carried out under in vivo conditions in [30], showed that it was very different from one cancer breast to another. This fact motivate us to take different values for the thermal conductivity as shown in Tab. 2. Moreover, in the experimental observations made in [30], the local temperature in cancerous breasts exhibited a bell-shaped profile, probably reflecting the increase of heat from the tumor. The increase of temperature and blood flow in and around the tumor seem to be well correlated, that is, the greater the blood supply to a tissue, the greater will be the heat produced. Therefore, the cancerous region can be considered as a heat source compared with the surrounding tissues, due to its higher metabolic rate. In particular, the metabolic heat generation (q_m^t) appears to be typical for each cancer and is very high in comparison with that of healthy breast tissue [30]. Higher values of q_m^t are generally associated to younger and smaller lesions [28].

In what follows, numerical results show a comparison among the two models A and B. We remark that tissue parameters given in [29] and [9] were also considered, however numerical results were similar to those presented and thus are not shown. First, Fig. 2 shows the temperature distribution of a healthy breast. We observe that the temperature is symmetrically distributed about the x_1 axis and it gradually decreases from the chest wall to the front breast area. Now, a sphere with radius $r = 0.01$ m was embedded in the breast model to mimic

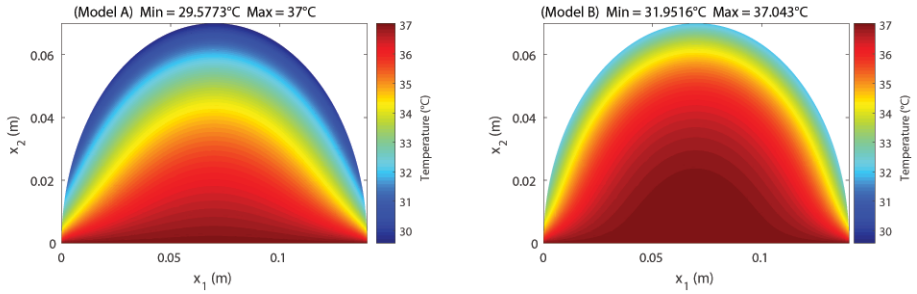

Figure 2: Temperature distribution of a healthy breast tissue.

the *in situ* tumor at a depth of $d = 0.02$ m (in the present study the depth is defined as the distance between the tumor center and the point on the breast surface in the same axis). In particular, a relative large tumor volume fraction $|Y_t| = 0.7$ is considered so that healthy breast tissue volume fraction is $|Y_g| = 0.3$ in the cancerous region. In Fig. 3 the temperature distribution of the cancerous breast tissue is presented. Clearly, thermal distribution varies

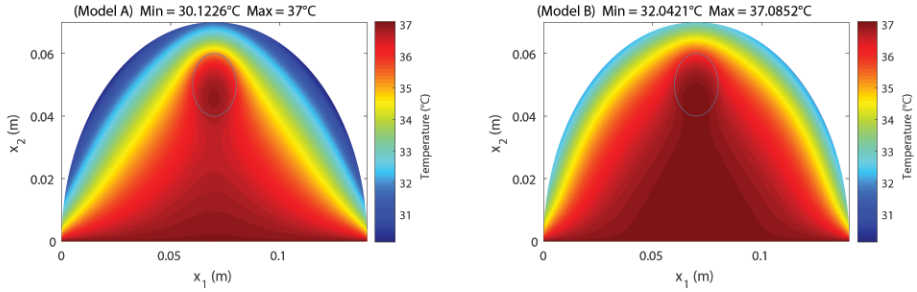

Figure 3: Temperature distribution of a cancerous breast tissue with an embedded spherical tumor of radius $1cm$. The solid line represents the boundary of the heterogeneous tumor.

from Fig. 2 to Fig. 3. That is, an anomaly in the region where the tumor is located and in the breast surface portion near to the tumor location is appreciated. As remarked by [29], an abnormal thermogram is a reliable indicator of high risk breast cancer and can also be of help in the differential diagnosis of benign from malignant tumors. In Fig. 4 is estimated the tumor-induced temperature alteration ($\Delta u = u_{tumor} - u_{healthy}$) between a cancerous and healthy breast, where u_{tumor} and $u_{healthy}$ are the temperature distributions on the cancerous and normal breast, respectively. Fig. 4 (Model A) shows a temperature variation of approximately 4℃ in the tumor area and the region surrounding it. Furthermore, in Fig. 4 (Model B) the variation is approximately 2℃. Also, in the zone "far" from the tumor area, no appreciable temperature changes are observed. This phenomenon is characteristic of tissues or organs with high metabolic rates, which consequently produce a large amount of heat. This reaction can

be explained because the greater the blood supply to a tissue, the greater the local metabolism and the greater is the local quantity of heat produced.

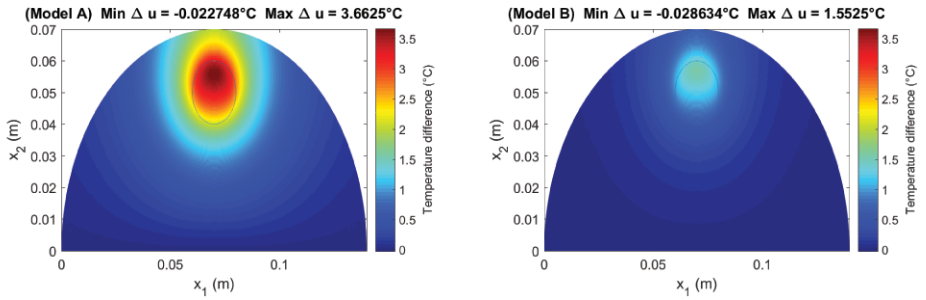

Figure 4: Estimated tumor-induced temperature alteration ($\Delta u = u_{tumor} - u_{healthy}$) between a cancerous and healthy breast.

Thermography only measures the breast surface temperature. Its core assumption is to find local surface temperature anomalies that points to a probable tumor site. From the thermal profile in Figs. 2-3, the surface temperature shows an anomaly. Indeed, Fig. 9 shows the surface temperature difference (Δu_s) between a healthy and a cancerous breast. It can be noticed that

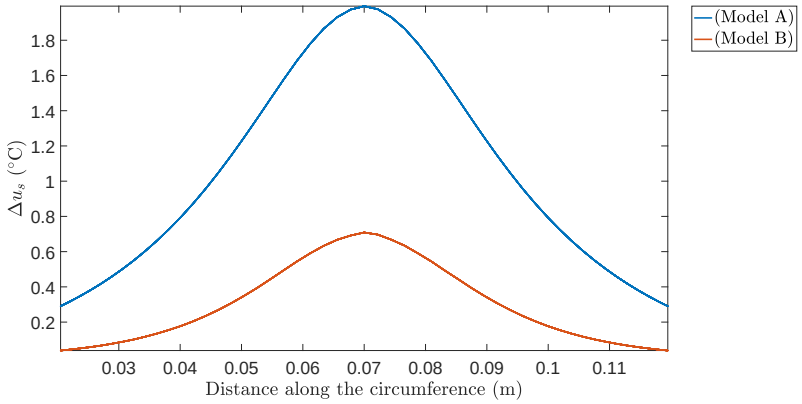

Figure 5: Estimated breast surface temperature difference (Δu_s) between a cancerous and healthy breast.

for the parameters values given in [3] (Fig. 5 (Model A)), the surface temperature difference is more meaningful. This behavior is a consequence of the blood perfusion rate values of the glandular tissue, i.e. as the perfusion rate of the glandular tissue for model A is lower than that from model B, the surface temperature difference in model A is higher than the corresponding to model B. These results agree with those obtained by [29].

6.1. Influence of tumor volume fraction on breast surface temperature

It is well known that tumor location influences the breast tissue temperature field [10, 29]. Indeed, as the tumor is closer to the boundary, the breast surface temperature increases. In the present work, we also show that having a composite material approach is significant to the temperature distribution. As shown in Fig. 10, we find that the cancer volume fraction degree in the malignant region affects the breast surface temperature. It is clear that a larger cancerous tissue volume fraction, produces a temperature rise and the opposite occurs when the

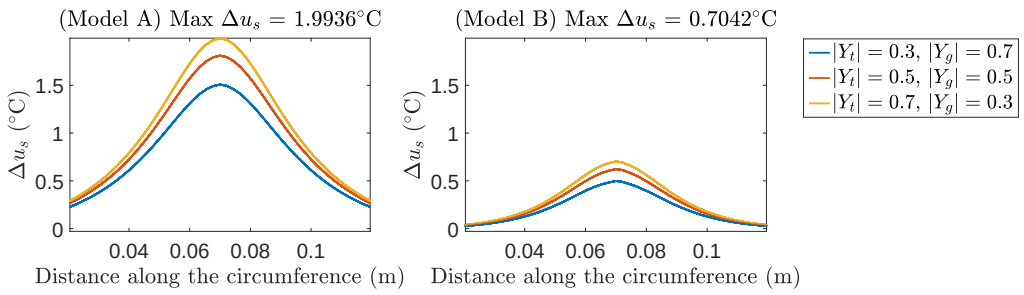

Figure 6: Estimated breast surface temperature difference (Δu_s) between a cancerous and healthy breast for different tumoral inclusions volume fraction.

tumor volume fraction diminishes. Then, assuming that the cancerous region is heterogeneous, extra information regarding thermal profile at the surface near the tumor is obtained. We note that although thermal properties for the tumor and glandular tissue in the malignant region in [3] are equal, the tumoral inclusions volume fraction affects the breast surface temperature. Increasing evidence shows that drug response is significantly reduced with increasing cell density [31]. Moreover, target volumes for radiotherapy is vital to its successful execution and requires the best possible characterization of the location and extent of tumor. In fact, the choice of radiotherapy dose depends on cell density where tumor control requires a higher dose if the initial cancerous cell number is larger [32]. Then, results shown in Fig. 6, provide a possible utility of thermal images to deduce the tumor volume percent in a determined tissue region and therefore adjust treatments.

6.2. Parameter sensitivity analysis

Now, the maximum temperature change on the breast surface Δu_s with respect to the tumor size and depth is illustrated in Fig. 7. In particular, it is elucidated that tumor depth has a

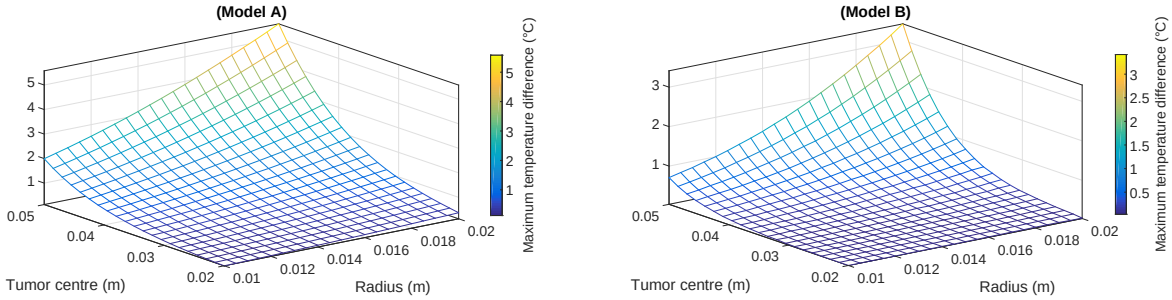

Figure 7: Estimated maximum surface temperature difference between normal and cancerous breasts as a function of tumor size and depth.

greater effect than tumor size on the tumor-induced temperature difference. Then, tumors closer to the surface will affect its temperature more prominently. This behavior agrees with the results obtained by [29] and [10]. Indeed, as the tumor gets closer to the surface, the maximum surface temperature difference increases. From the numerical results, this change is more evident for tumors with center in the interval $[0.03, 0.05]$ (Figs. 7 (Model A)) and $[0.04, 0.05]$ (Fig. 7 (Model B)). Furthermore, surface temperature change Δu_s is plotted with respect to tumor size and tumoral volume fraction and presented in Fig. 8. We notice (as

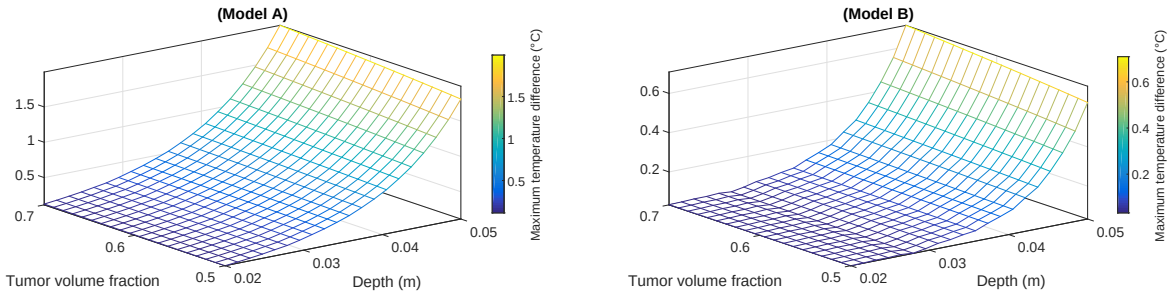

Figure 8: Estimated maximum surface temperature difference between normal and cancerous breasts as a function of tumor size and volume fraction.

expected) that tumor size influences more the temperature change Δu_s than tumoral volume fraction. Consequently, tumor depth still has a greater effect on the breast surface temperature.

6.3. Comparison with experimental data

The model results are compared with the experimental data given in [30]. Following [30], we have fixed $h = 10$ W/m ℃, $u_c = 36$℃, $d = 0.48$ m and $r = 0.01$ m. In [3], a standardized protocol for the acquisition of breast thermal images is developed. In their study two room temperatures $u_e = 24.9$℃ and $u_e = 28$℃, are reported. Based on this fact, we fix $u_e = 26$℃. Figure 9 shows the comparison of the obtained computational results and the experimental

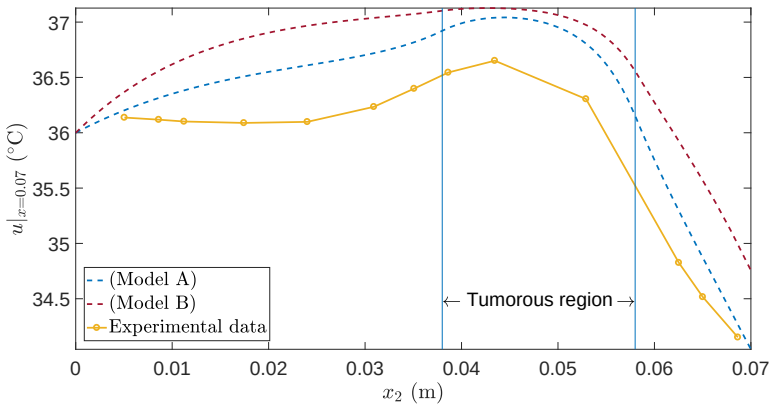

Figure 9: Comparison of numerical results from models A and B with the experimental data taken from [30].

data in [30]. We observe that though there is a quantitatively difference, there is a satisfactory qualitative match in the whole interval. Here we remark that for simplicity, we model the homogeneous tissue surrounding the tumor area comprised of only glandular tissue. As a matter of fact, breasts are also composed of a muscle layer and subcutaneous fat layer [9]. In this sense, adding more information to the model must (in principle) induce a more accurate agreement with the experimental data.

7. Conclusions

In this work, a semi-analyical approach is used for studying breast thermography through coupled stationary bioheat transfer equations. The breast is represented by two regions of dif-

ferent thermophysical properties: the glandular tissue and the tumor tissue. A two-dimensional cross-section of the average female breast geometry is considered and the tumor lesion is assumed to be an encapsulated and round heterogeneous tissue composed of both glandular and periodically arranged circular cancerous inclusions. The material thermal properties of matrix and inclusions are supposed isotropic. In particular, the temperature distribution on both, breast and tumor tissue, was computed using a numerical algorithm implemented in *FreeFem++*. In summary, we obtain that: (a) the tumor presence in a breast does affect its surface temperature distribution. Specially, it is higher on the surface close to the tumor. (b) Low perfusion rates of glandular tissue induce a higher temperature difference in the tumor region. (c) No appreciable changes in temperature difference were observed far from the tumor position. (d) Tumor depth has a greater effect than the tumor size and volume fraction on the maximum surface temperature difference. As the tumor moves closer to the surface, the maximum breast surface difference temperature increases. (e) The augment of the cancerous tissue volume fraction implies an increase in the breast surface temperature near the tumor. (f) A good qualitative agreement is observed between the model and experimental data.

Some future research directions that we intend to explore are the following. To consider the dynamic version of the considered bioheat equation with anisotropic thermal properties of the tumorous tissue. Besides, to contemplate breasts made from the combination of different tissue layers (fats, muscles, glands, veins and milk channels). Furthemore, a more realistic description of blood perfusion, which is driving temperature changes within the breast tissue, could be provided by accounting explicitly for the topology and hydraulic properties of the tumor microvasculature (see the works [33, 34], which is based on the multiscale models [35] and [26]). Finally, a three-dimensional setting could be conceived by using the results in [36, 37], as well as the implementation of a non-macroscopically uniform generalization of the model (see Remark 1) to account for realistic microstructures given by appropriate medical images.

The proposed approach provides a helpful framework for thermographic diagnosis and treatment of breast tumors. It facilitates the understanding of the complex mechanism underlying the observed surface temperature profile. Also, it improves the current early tumor detection and analysis of the thermography technique, integrating mathematical and computational tools (see e.g. [6]). In fact, infrared thermography has shown to be a promising noninvasive and effective adjunctive modality to X-ray mammography for breast cancer detection [8]. Moreover, it has great potential for earlier detecting cancer [3] and according to [4], this may happen years earlier than with other techniques. No single tool provides excellent predictability; however, a combination that incorporates thermography may boost both sensitivity and specificity.

Acknowledgements

AR, LP and AF are financially supported by INdAM. AR gratefully acknowledges the Program of Postdoctoral Scholarships of DGAPA from UNAM, Mexico. JM and RP acknowledges support from the Ministerio de Ciencia in Spain under the project reference DPI2014-58885-R. Thanks to the Project (7515) Métodos Físico-Matemáticos para el estudio de nuevos materiales y la propagación de ondas. Aplicaciones. AC is grateful to CNPq (Projects INCT-MACC and 303240/2015-6). The authors would like to thank Professor Sébastien Martin, Université Paris Descartes, Paris, France for helpful discussions during the course of this work. Also, we thanks to Departamento de Matemáticas y Mecánica IIMAS-UNAM for their support and Ramiro Chávez Tovar and Ana Pérez Arteaga for computational assistance.

Appendix A. Analytic solution of the cell problem

The cell problem is given by

$$\begin{cases} \frac{\partial^2 \chi_p^{(\gamma)}}{\partial y_i \partial y_j} = 0 & \text{in } Y \setminus \Gamma, \\ [\![\chi_p]\!] = 0 & \text{on } \Gamma, \\ [\![K_{ij} \frac{\partial \chi_p}{\partial y_j} n_i]\!] = -[\![K_{ip} n_i]\!] & \text{on } \Gamma, \end{cases} \tag{A.1}$$

where $i, j, p = 1, 2$ and $\gamma = g, t$. Then, the mathematical statement of the problem consists in finding doubly-periodic harmonic functions with null average over the periodic cell that satisfy the Laplace equation in (A.1). Consequently, the method of complex variables in terms of two harmonic functions $\varphi_p^{(\gamma)}(z)$ and $\psi_p^{(\gamma)}(z)$ and the Kolosov-Muskhelishvili complex potentials are applicable.

The complex potentials $\varphi_p^{(\gamma)}(z)$ and $\psi_p^{(\gamma)}(z)$ are looked for the periodic cell that contains the origin of coordinates in the following form

$$\varphi_p^{(g)}(z) = a_0^p z + \sum_{k=1}^{\infty\ o} a_k^p \frac{\zeta^{(k-1)}(z)}{(k-1)!} \quad \text{and} \quad \psi_p^{(t)}(z) = \sum_{k=1}^{\infty\ o} c_k^p z^k, \tag{A.2}$$

for the glandular and tumor phases, respectively. In (A.2), a_k^p and c_k^p are real coefficients to be determined, ζ represents the quasi-periodic Weierstrass functions of periods $w_1 = 1$ and $w_2 = i$, $\zeta^{(k)}$ denotes the k^{th} derivative of ζ which are doubly-periodic functions of z and the superscript o specifies that the sum is carried out over odd indices. Now, using Legendre's relations, periodicity conditions for $\varphi_p^{(g)}$ are satisfied if

$$a_0^p = (-1)^p a_1^p \pi. \tag{A.3}$$

Moreover, the Laurent series of $\zeta^{(k-1)}$ (for $k \geq 0$ and k odd) in zero is given by

$$\frac{\zeta^{(k-1)}}{(k-1)!} = \frac{1}{z^k} - \sum_{l=1}^{\infty\ o} k \eta_{kl} z^l \quad \text{with } \eta_{kl} = \frac{(k+l-1)!}{k!l!} S_{k+l}, \tag{A.4}$$

where S_k are the reticulate sums; they are defined as $S_k = \sum_{w \in L^*} \frac{1}{w^k}$ ($k \geq 3$, k odd) with $w = mw_1 + nw_2$ where $m, n \in \mathbb{Z}$ and L^* represents the lattice excluding $w = 0$. Using formulas (A.3), (A.4) and defining $\eta_{11} = (-1)^{p+1}\pi$,

$$\varphi_p^{(g)}(z) = \sum_{l=1}^{\infty\ o} \left(a_l^p z^{-l} - A_l^p z^l \right) \quad \text{with } A_l^p = \sum_{k=1}^{\infty\ o} k a_k^p \eta_{kl}. \tag{A.5}$$

Case $p = 1$: The following *ansatz* is proposed,

$$\chi_1^{(g)} = \mathcal{R}\left(\varphi_1^{(g)}\right) = \mathcal{R}\left(\sum_{l=1}^{\infty\ o} \left(a_l^1 z^{-l} - A_l^1 z^l \right) \right) \quad \text{and} \quad \chi_1^{(t)} = \mathcal{R}\left(\psi_1^{(t)}\right) = \mathcal{R}\left(\sum_{l=1}^{\infty\ o} c_l^1 z^l \right), \tag{A.6}$$

where $\mathcal{R}$ defines the real part of the involved function. Here, it is noticed that $\Gamma = Re^{i\theta}$ where R is the radius of the circular inclusion. Then,

$$\chi_1^{(g)} = \sum_{l=1}^{\infty\ o} \left(a_l^1 R^{-l} - A_l^1 R^l\right) \cos\theta l \quad \text{and} \quad \chi_1^{(t)} = \sum_{l=1}^{\infty\ o} c_l^1 R^l \cos\theta l. \tag{A.7}$$

Substituting the last expression into the first boundary condition of (A.1), we have for all l odd,

$$a_l^1 R^{-l} - A_l^1 R^l = c_l^1 R^l. \tag{A.8}$$

On the other hand, substituting (A.7) in the second boundary condition of (A.1) and after several manipulations, it is obtained for all l odd,

$$a_l^1 R^{-l} + \xi A_l^1 R^l = \xi R^l \delta_{1l}, \tag{A.9}$$

where δ_{ij} is Kronecker's delta and $\xi = \frac{k_g - k_t}{k_g + k_t}$. Now, re-scaling with $a_l^1 = \frac{\hat{a}_l^1 R^l}{\sqrt{l}}$, equation (A.9) can be written as an infinite linear system in the form

$$\left(\boldsymbol{I} + \xi \boldsymbol{W}^1\right) \hat{\boldsymbol{A}}^1 = \boldsymbol{V}^1, \tag{A.10}$$

where $\hat{\boldsymbol{A}}^1 = (a_1^1, a_2^1, \ldots)^T$, $\boldsymbol{V}^1 = (\xi R, 0, \ldots)$ and

$$\boldsymbol{W}^1 = \begin{cases} \pi R^2 & \text{for } k+l = 2, \\ \sum_{k=1}^{\infty\ o} \sqrt{kl}\,\eta_{kl} R^{k+l} & \text{for } k+l > 2. \end{cases}$$

Case $p = 2$: The following *ansatz* is proposed,

$$\chi_2^{(g)} = \mathcal{I}\left(\varphi_2^{(g)}\right) = \mathcal{I}\left(\sum_{l=1}^{\infty\ o} \left(a_l^2 z^{-l} - A_l^2 z^l\right)\right) \quad \text{and} \quad \chi_2^{(t)} = \mathcal{I}\left(\psi_2^{(t)}\right) = \mathcal{I}\left(\sum_{l=1}^{\infty\ o} c_l^2 z^l\right), \tag{A.11}$$

where $\mathcal{I}$ defines the imaginary part of the involved function. As for $p = 1$, the following infinite linear system is obtained

$$\left(\boldsymbol{I} - \xi \boldsymbol{W}^2\right) \hat{\boldsymbol{A}}^2 = \boldsymbol{V}^2, \tag{A.12}$$

where $\hat{\boldsymbol{A}}^2 = (a_1^2, a_2^2, \ldots)^T$, $\boldsymbol{V}^2 = (-\xi R, 0, \ldots)$ and

$$\boldsymbol{W}^2 = \begin{cases} -\pi R^2 & \text{for } k+l = 2, \\ \sum_{k=1}^{\infty\ o} \sqrt{kl}\,\eta_{kl} R^{k+l} & \text{for } k+l > 2. \end{cases}$$

References

[1] American Cancer Society, Breast Cancer Facts & Figures 2015-2016., American Cancer Society, Incdoi:10.1093/med/9780199363315.003.0020.

[2] D. Kennedy, T. Lee, D. Seely, A comparative review of thermography as a breast cancer screening technique., Integrative cancer therapies 8 (1) (2009) 9–16. doi:10.1177/1534735408326171.

[3] L. A. Bezerra, M. M. Oliveira, T. L. Rolim, A. Conci, F. G. S. Santos, P. R. M. Lyra, R. C. F. Lima, Estimation of breast tumor thermal properties using infrared images, Signal Processing 93 (10) (2013) 2851–2863. doi:10.1016/j.sigpro.2012.06.002.
URL http://dx.doi.org/10.1016/j.sigpro.2012.06.002

[4] J. R. Keyserlingk, P. D. Ahlgren, E. Yu, N. Belliveau, M. Yassa, Functional infrared imaging of the breast., IEEE Engineering in Medicine and Biolgy Magazine 19 (3) (2000) 30–41.
URL http://www.ncbi.nlm.nih.gov/pubmed/?term=10834114

[5] P. Kapoor, S. V. a. V. Prasad, Image processing for early diagnosis of breast cancer using infrared images, The 2nd International Conference on Computer and Automation Engineering (ICCAE) 3 (2010) 564–566. doi:10.1109/ICCAE.2010.5451827.
URL http://ieeexplore.ieee.org/lpdocs/epic03/wrapper.htm?arnumber=5451827

[6] L. F. Silva, A. A. S. M. D. Santos, R. S. Bravo, A. C. Silva, D. C. Muchaluat-Saade, A. Conci, Hybrid analysis for indicating patients with breast cancer using temperature time series, Computer Methods and Programs in Biomedicine 130 (2016) 142–153.

[7] J. F. Head, R. L. Elliott, Infrared imaging: Making progress in fulfilling its medical promise, IEEE Engineering in Medicine and Biology Magazine 21 (6) (2002) 80–85. doi:10.1109/MEMB.2002.1175142.

[8] E. Y. K. Ng, A review of thermography as promising non-invasive detection modality for breast tumor, International Journal of Thermal Sciences 48 (5) (2009) 849–859. doi:10.1016/j.ijthermalsci.2008.06.015.

[9] A. A. Wahab, M. I. M. Salim, M. A. Ahamat, N. A. Manaf, J. Yunus, K. W. Lai, Thermal distribution analysis of three-dimensional tumor-embedded breast models with different breast density compositions, Medical and Biological Engineering and Computing (2015) 1–11doi:10.1007/s11517-015-1403-7.

[10] L. Jiang, W. Zhan, M. H. Loew, Modeling static and dynamic thermography of the human breast under elastic deformation., Physics in Medicine and Biology 56 (1) (2011) 187–202. doi:10.1088/0031-9155/56/1/012.

[11] K. Das, R. Singh, S. C. Mishra, Numerical analysis for determination of the presence of a tumor and estimation of its size and location in a tissue, Journal of Thermal Biology 38 (1) (2013) 32–40. doi:10.1016/j.jtherbio.2012.10.003.
URL http://dx.doi.org/10.1016/j.jtherbio.2012.10.003

[12] R. Penta, D. Ambrosi, R. J. Shipley, Effective governing equations for poroelastic growing media, Quarterly Journal of Mechanics and Applied Mathematics 67 (1) (2014) 69–91. doi:10.1093/qjmam/hbt024.

[13] E. Sanchez-Palencia, Non-Homogeneous Media And Vibration Theory, Vol. 127, Springer-Verlag, Berlin, 1980. doi:10.1007/3-540-10000-8.
URL http://adsabs.harvard.edu/abs/1980LNP...127.....S

[14] N. Bakhalov, G. Panasenko, Homogenisation: Averaging Processes in Periodic Media, Kluwer Academic Publishers, Dordrecht, 1989. doi:10.1007/978-94-009-2247-1.

[15] R. Guinovart-Díaz, J. C. López-Realpozo, R. Rodríguez-Ramos, J. Bravo-Castillero, M. Ramírez, H. Camacho-Montes, F. J. Sabina, Influence of parallelogram cells in the axial behaviour of fibrous composite, International Journal of Engineering Science 49 (1) (2011) 75–84. doi:10.1016/j.ijengsci.2010.06.024.

[16] F. J. Sabina, R. Guinovart-Díaz, R. Rodríguez-Ramos, J. C. López-Realpozo, J. Bravo-Castillero, Overall properties in fibrous elastic composite with imperfect contact condition, International Journal of Engineering Science 61 (2012) 142–155. doi:10.1016/j.ijengsci.2012.06.017.
URL http://dx.doi.org/10.1016/j.ijengsci.2012.06.017

[17] H. Pennes, Analysis of tissue and arterial blood temperatures in the resting human forearm, Journal of Applied Physiology 1 (2) (1948) 93–122.

[18] Y. Jayasinghe, P. S. Simmons, Fibroadenomas in adolescence, Current Opinion in Obstetrics and Gynecology 21 (2009) 402–406. doi:10.1097/GCO.0b013e32832fa06b.

[19] R. M. Youngson, Collins Dictionary of Medicine, HarperCollins, 1992.

[20] Y.-T. Wu, S.-T. Chen, C.-J. Chen, Y.-L. Kuo, L.-M. Tseng, D.-R. Chen, S.-J. Kuo, H.-W. Lai, Breast cancer arising within fibroadenoma : collective analysis of case reports in the literature and hints on treatment policy, World Journal of Surgical Oncology 12 (2014) 1–8.

[21] H. Abe, K. Hanasawa, H. Naitoh, Y. Endo, T. Tani, R. Kushima, Invasive ductal carcinoma within a fibroadenoma of the breast, International Journal of Clinical Oncology 9 (2004) 334–338. doi:10.1007/s10147-004-0401-9.

[22] M. Kurosumi, R. Itokazu, Y. Mamiya, K. Kishi, S. Takayama, lnvasive ductal carcinoma with a predominant intraductal component arising in a fibroadenoma of the breast, Pathology International 44 (July) (1994) 874–877.

[23] M. Salhab, L. G. Keith, M. Laguens, W. Reeves, K. Mokbel, International Seminars in Surgical The potential role of dynamic thermal analysis in breast cancer detection, International Seminars in Surgical Oncology 5 (2006) 1–5. doi:10.1186/1477-7800-3-8.

[24] R. Burridge, J. Keller, Poroelasticity equations derived from microstructure, Journal of acoustical society of America 70 (1981) 1140–1146.

[25] M. Holmes, Introduction to perturbation method, Springer-Verlag, 1995.

[26] R. Penta, D. Ambrosi, A. Quarteroni, Multiscale homogenization for fluid and drug transport in vascularized malignant tissues, Mathematical Models and Methods in Applied Sciences 25 (01) (2015) 79–108. doi:10.1142/S0218202515500037.
URL http://www.worldscientific.com/doi/abs/10.1142/S0218202515500037

[27] N. I. Muskhelishvili, Some Basic Problems of the Mathematical Theory of Elasticity, Springer Netherlands, 1977. doi:10.1007/978-94-017-3034-1.

[28] F. Bardati, S. Iudicello, Modeling the visibility of breast malignancy by a microwave radiometer, IEEE Transactions on Biomedical Engineering 55 (1) (2008) 214–221. doi:10.1109/TBME.2007.899354.

[29] A. Amri, A. Saidane, S. Pulko, Thermal analysis of a three-dimensional breast model with embedded tumour using the transmission line matrix (TLM) method, Computers in Biology and Medicine 41 (2) (2011) 76–86. doi:10.1016/j.compbiomed.2010.12.002.
URL http://dx.doi.org/10.1016/j.compbiomed.2010.12.002

[30] M. Gautherie, Thermopathology of Breast Cancer : Measurement and Analysis, Annals of the New York Academy of Sciences (1980) 383–415.

[31] M. Hakanson, S. Kobel, M. P. Lutolf, M. Textor, E. Cukierman, M. Charnley, Controlled breast cancer microarrays for the deconvolution of cellular multilayering and density effects upon drug responses, PLoS ONE 7 (6). doi:10.1371/journal.pone.0040141.

[32] N. G. Burnet, S. J. Thomas, K. E. Burton, S. J. Jefferies, Defining the tumour and target volumes for radiotherapy, Cancer Imaging 4 (2) (2004) 153–161. doi:10.1102/1470-7330.2004.0054.

[33] R. Penta, D. Ambrosi, The role of the microvascular tortuosity in tumor transport phenomena, Journal of Theoretical Biology 364 (2015) 80–97. doi:10.1016/j.jtbi.2014.08.007.
URL http://dx.doi.org/10.1016/j.jtbi.2014.08.007

[34] P. Mascheroni, R. Penta, The role of the microvascular network structure on diffusion and consumption of anticancer drugs, International Journal for Numerical Methods in Biomedical Engineering (2017) e2857–n/aE2857 cnm.2857. doi:10.1002/cnm.2857.
URL http://dx.doi.org/10.1002/cnm.2857

[35] R. J. Shipley, S. J. Chapman, Multiscale modelling of fluid and drug transport in vascular tumours, Bulletin of Mathematical Biology 72 (6) (2010) 1464–1491. doi:10.1007/s11538-010-9504-9.

[36] R. Penta, A. Gerisch, Investigation of the potential of asymptotic homogenization for elastic composites via a three-dimensional computational study, Computing and Visualization in Science 17 (4) (2015) 185–201. doi:10.1007/s00791-015-0257-8.
URL http://link.springer.com/10.1007/s00791-015-0257-8

[37] R. Penta, A. Gerisch, The asymptotic homogenization elasticity tensor properties for composites with material discontinuities, Continuum Mechanics and Thermodynamics 29 (1) (2017) 187–206.